JOURNAL OF APPLIED ELECTROCHEMISTRY **28** (1998) 1141–1145

Bubble coverage and bubble resistance using cells with horizontal electrode

K. QIAN, Z. D. CHEN*, J. J. J. CHEN

Department of Chemical & Materials Engineering, The University of Auckland, Private Bag 92019, Auckland, New Zealand

Received 29 January 1998; accepted in revised form 17 March 1998

The resistivity ratio due to gas bubbles underneath horizontal anodes in electrolytic cells was measured and compared with that in an air–water model of identical geometry. It was found that at equal current density or equivalent gas generation rate, the difference in the bubble resistivity ratio between these two situations can be up to 20%. Consequently, the results obtained from an air–water model cannot be directly applied to an electrolytic cell. Results also showed that within the range of experimental conditions covered, the bubble resistivity ratios obtained for a given anode–cathode distance in both cells are linearly related to the bubble coverage ratio, based on bubbles greater than a certain size as limited by the measurement method.

Keywords: *bubble coverage*, *bubble resistivity*, *electrolytic cells*, *horizontal electrode*

List of symbols

a	intercept of the best fit line on the ordinate
L_{AC}	anode–cathode distance (m)
b	slope of the best-fit line
j	current density (A cm^{-2})
d	bubble diameter (mm)
f	bubble coverage ratio
i	bubble group number
m_i	measured number of bubbles in group i
n	anode–cathode distance (cm)
R	resistivity ratio, ρ_{eff}/ρ_0
$\Delta a_{n\,cm}$	additional bubble resistivity ratio for the electrolytic cell with an ACD of n cm at zero bubble coverage ratio when compared with that of the air–water model.
$\Delta R_{n\,cm}$	total resistivity ratio increase for the electrolytic cell with an ACD of n cm due to the existence of the bubble layer under the anode.
ρ	resistivity (Ω m)

Subscripts

0	with no bubble present
eff	effective, or, with bubbles present
exp	experimental
ncm	with ACD of n cm

1. Introduction

The evaluation of resistivity ratio due to the presence of gas bubbles under horizontal electrodes is one of the important problems encountered in electrochemical technology, for example, in the production of aluminium using Hall–Héroult cells. Although results obtained from actual reduction cells have been reported by several researchers [1–3], accurate measurements of bubble resistance in cells operating at elevated temperatures are nearly impossible due to the difficulties in isolating the various resistance components. A number of investigations were carried out using either air–water (often with additives) physical analogue models [4–6] or small-scale electrolytic cells [7–9]. In a previous paper [10], it was shown that the bubble behaviour in an air–water physical analogue model (AWM) was significantly different from those in an electrolytic cell due to the different bubble generation mechanisms. On the one hand, bubbles formed in an air–water model by forcing air through porous plate are larger and has clear wetted areas between bubbles. On the other hand, electrolytically generated bubbles are smaller and the electrode surface is covered with fine bubbles which appear foamy. Consequently, it was suggested that the bubble resistivity ratio obtained from an air–water model cannot be directly applied to an electrolytic cell.

The additional resistance due to the presence of gas bubbles is influenced by the behaviour of bubbles under the electrode which may be characterized by various parameters such as bubble velocity, bubble size, bubble shape, bubble layer thickness, bubble coverage ratio, bubble void fraction, bubble distribution etc. It is possible that, for a given situation, not all of these parameters need to be determined to characterise the resulting bubble resistance. Previous

* Author to whom correspondence should be addressed.

investigations [11–13] on vertical electrode cells have shown that the bubble resistance is determined by the bubble void fraction in the electrolyte in the interpolar region. Sides and Tobias [14] showed that the same relationship applies also to horizontal electrode cells in the region of the gas bubble layer underneath the electrode surface if the bubbles have a wide range of sizes.

A number of correlations suggested for the bubble resistivity ratio in aluminium reduction cells involve the bubble void fraction [1, 5, 13, 15]. It should be noted that in these works concerning horizontal electrodes, the measurement method for gas void fraction was inadequate except that of Sides and Tobias [14] who used discrete solid spheres to simulate the bubbles. In cells with vertical electrodes, bubbles are dispersed in the interpolar region and the average void fraction of the gas bubbles can be easily obtained by measuring the change in the height of the electrolyte before and during electrolysis. However, in cells with horizontal electrodes, a significant number of the bubbles are outside the interpolar region, when the bubbles evacuate from the anode bottom and rise to the electrolyte free surface. Consequently, the void fraction measurements by considering changes in the height of the electrolyte is inappropriate and the validity of the correlations which require the bubble void fraction is thus questionable.

Further, the application of correlations based on physical analogue models such as that suggested by Solheim and Thonstad [5] is in question since the bubble behaviour in these models is significantly different from those in actual electrolytic cells as shown by Qian *et al.* [10].

In this work, bubble resistivity ratio for an electrolytic cell was measured and compared with that of an air–water model with the same geometry. In addition, the relationship between the bubble coverage ratio on the anode surface and the bubble resistivity ratios for both the air–water model and the electrolytic cell were investigated.

2. Experimental details

Details of the air–water model (AWM) and the electrolytic cell used in this work have been reported in a previous paper [10] and only a brief description will be given here. For the AWM shown schematically in Fig. 1, the simulated anode with the bottom surface made of porous bronze plate had a working area of 100 mm × 40 mm. The bubbles under the simulated anode were generated by forcing compressed air through the porous bronze plate. Two plexiglass side plates of area 60 mm × 100 mm, completely bounded the two 100 mm sides of the simulated anode and the bottom edge of the side plates was 10 mm below the working area of the simulated anode. Experiments were conducted using tap water at room temperature between 18 °C and 25 °C.

Figure 2 shows a schematic view of the electrolytic cell. Two types of anode were used: one machined from a graphite block and the other made from a spent carbon anode from an industrial aluminium reduction cell with the working surface in the as-received after-service condition. The working surface area of both anodes and the side plates had the same dimensions as those used in the AWM. When using the graphite anode, the electrolytic cell will be referred to as ECG and when the carbon anode was used, it will be referred to as ECC.

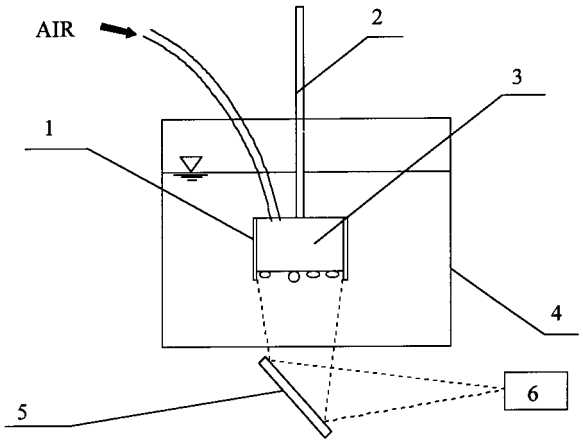

Fig. 1. Schematic diagram of the air–water model (AWM): (1) side plates; (2) support rod; (3) simulated anode; (4) tank; (5) mirror; (6) video.

A split graphite cathode, consisting of two blocks of graphite placed on either side of the anode, was used to allow observations of the bubble behaviour from a position directly below the anode. A 2 M NaOH solution was used as the electrolyte. Due to the energy input by the current, the temperature of the electrolyte was in the range 46 ± 3 °C. Two screens above the split cathode were used to direct the bubbles generated on the cathode in order to minimize their influence on the flow field, the resistivity measurement and the visual observation.

The bubble resistance was measured by a method using the fast Fourier transformation (FFT) of the fluctuating voltage signals due to an imposed a.c. signal which had been detailed in a previous paper [10].

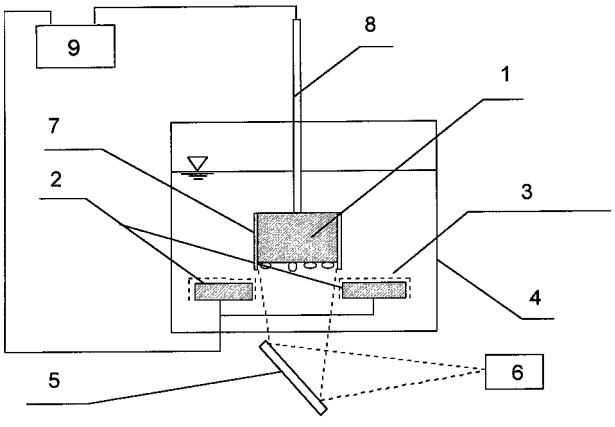

Fig. 2. Schematic diagram of the electrolytic cell: (1) top electrode; (2) split bottom electrodes; (3) screen; (4) tank; (5) mirror; (6) video; (7) side plates; (8) support rod; (9) d.c. power supply.

With reference to Figs 1 and 2, a plan view of the bubbles on the bottom-facing anode was recorded by a video camera via a mirror placed below the tank and inclined at 45°. The recordings were then played back and measurements were made directly on a video monitor. Due to problems associated with clearly defining the bubbles on the video monitor, only bubbles greater than 0.8 mm in diameter were considered.

For the AWM, bubbles were categorized into twelve groups based on the following diameter ranges: 0.8–2, 2–4, 4–6, 6–8, 8–10, 10–12, 12–14, 14–16, 16–18, 18–20, 20–22 and 22–24 mm. Average diameters of 1.4, 3, 5, 7, 9, 11, 13, 15, 17, 19, 21 and 23 mm were used to calculate the bubble coverage ratio for each group of bubbles. A set of 10 repeat samples were taken at an interval of 0.5 s to evaluate the average bubble coverage ratio.

Bubbles for the electrolytic cell were divided into two types: large (diam. > 0.8 mm) and fine (diam. < 0.8 mm). Most of the fine bubbles were found interspersed between the large bubbles, while a certain proportion may be dispersed into the electrolyte but close to the anode surface. Large bubbles were all found adhering to the underside of the anode. These two types of bubbles are expected to have different effects on the bubble resistance. The video recordings of the bubbles during tests were played back and the number of bubbles larger than 0.8 mm diameter (large bubbles) were counted and grouped using the same method as that for the AWM.

From the diameter measurements, the bubble coverage ratio on the anode which measures 40 mm × 100 mm can be evaluated:

$$f = \frac{\sum_{i=1}^{12} m_i \times \frac{\pi d_i^2}{4}}{40 \times 100} \quad (1)$$

where i is the bubble group number, d_i (mm) the average bubble diameter in group i and m_i the measured number of bubbles in group i.

Since Equation 1 involves only bubbles larger than 0.8 mm in diameter, its application to the AWM includes essentially all the bubbles present. However, for the electrolytic cell, fine bubbles have not been taken into account in the bubble coverage.

3. Results and discussion

3.1. *Comparison of the bubble resistance ratio between the air–water model and the electrolytic cell*

The bubble coverage ratio and bubble resistivity ratio for the AWM, ECG and ECC were measured for electrode inclinations of 2°, 4°, 6° and 8°, current densities (j) of 0.45, 0.60 and 0.75 A cm^{-2} and anode–cathode distance (L_{AC}) of 1, 2, 3, 4, 5 and 6 cm. Figure 3 gives a plot of the ratio of the resistivity ratio for the AWM to that for the ECG at L_{AC} = 1 cm ($R_{AWM,\,1\,cm}/R_{ECG,\,1\,cm}$), against the current density. Since the values for the ECG and ECC are very close to each other, the data for the ECC have not been included.

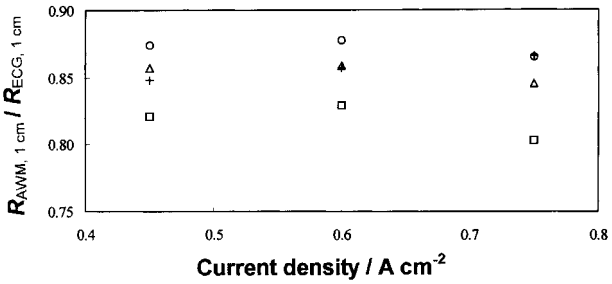

Fig. 3. Ratio of the resistivity ratio for the AWM to that for the ECG at L_{AC} = 1 cm ($R_{AWM,\,1\,cm}/R_{ECG,\,1\,cm}$), against the gas generation rate or current density. Key: (○) 2°, (+) 4°, (△) 6° and (□) 8°.

It is seen that at equal current density or equivalent gas generation rate, the bubble resistivity ratio for the AWM is significantly lower than that for the ECG. The maximum difference of the bubble resistivity ratio under the same anode inclination can be up to 20%, which suggests that the results obtained from an air–water model cannot be directly applied to an electrolytic cell.

As shown in a previous paper [10], at equal density or equivalent gas generation rate, the average bubble size on the anode in the ECG and the ECC is significantly smaller than that for the AWM. Consequently, the bubbles in the ECG and ECC move at a lower velocity and the residence time for the gas under the anode is therefore greater. This leads to higher gas void fraction in the bubble layer under the anode. According to Sides and Tobias [14], high gas void fraction of the bubble layer gives rise to high bubble resistance. This explains the high resistivity ratio for the ECG and the ECC compared to the AWM.

3.2. *Relationship between bubble coverage ratio and bubble resistivity ratio*

The relationship between the bubble coverage ratio and the bubble resistivity ratio in the AWM, the ECG and the ECC for an ACD of 1 cm with the electrode inclinations of 2°, 4°, 6° and 8° j = 0.45, 0.60 and 0.75 A cm^{-2} are shown in Fig. 4. It is seen that within the experimental conditions covered in this work, the

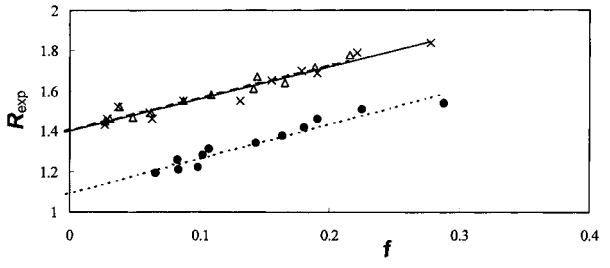

Fig. 4. Bubble resistivity ratio against bubble coverage ratio at L_{AC} = 1 cm for the AWM (●), ECG (△) and ECC (×) with j = 0.45, 0.60 and 0.75 A cm^{-2} and electrode inclinations of 2°, 4°, 6° and 8°. Key: (· · · · ·) best fit (AWM), (- - - -) best fit (ECG) and (——) best fit (ECC).

bubble resistivity ratios for the AWM, the ECG and the ECC are linearly related to the bubble coverage ratios. The linear relationship between the bubble resistivity ratio, $R_{1\,cm}$ and the bubble coverage ratio, f, at an ACD of 1 cm may by represented by the following equation:

$$R_{1cm} = a_{1cm} + b_{1cm} f \tag{2}$$

where $a_{1\,cm}$ and $b_{1\,cm}$ are the intercept on the ordinate and the slope of the best fit line for $L_{AC} = 1$ cm.

Table 1 lists the values of $a_{1\,cm}$ and $b_{1\,cm}$ for the AWM, ECG and ECC, respectively. It is seen that the slope of the best fit lines remains effectively constant, independent of whether it is the air–water model or the electrolytic cell, and in the case of the electrolytic cell, it is also independent of whether graphite anode or carbon anode was used. The intercepts on the ordinate for ECG and ECC are effectively the same, but is significantly different from that of AWM. With the AWM, it would normally be expected that at zero bubble coverage, the resistivity ratio should be 1.0. It is seen that the deviation of the intercept from 1.0 is, in fact, very small.

Based on the relationship of the bubble resistivity ratio and the bubble coverage ratio at $L_{AC} = 1$ cm, it is possible to predict the bubble resistivity ratio for other anode–cathode distances. Since the thickness of the bubble layer under the anode is less than 1 cm and no bubble exists in the interpolar region 1 cm away from the anode surface, the effective resistivity of the electrolyte 1 cm away from the anode should not be or should only be slightly affected by the existence of the bubble layer. Consequently, the bubble resistivity ratio $R_{n\,cm}$ at $L_{AC} = n$(cm) can be approximated by the equation:

$$R_{\text{Eq. (3), } n\,cm} = \frac{(a_{1cm} + b_{1cm} f)\rho_0 + (n-1)\rho_0}{n\rho_0} = \frac{a_{1cm} + n - 1}{n} + \frac{b_{1cm} f}{n} \tag{3}$$

Equation 3 indicates that the bubble resistivity ratio $R_{n\,cm}$ at any given anode–cathode distance should also be a linear function of the bubble coverage ratio. Figure 5 shows a comparison between the predictions by Equation 3 and the experimental results obtained for the AWM, ECG and ECC with electrode inclinations of 2°, 4°, 6° and 8°, $j = 0.45$, 0.60 and 0.75 A cm^{-2} and $L_{AC} = 2$, 3, 4, 5 and 6 cm. It is seen that the predictions are in good agreement with the experimental results with a maximum deviation of 2.7%.

3.3. *Effects of fine bubbles*

The effect of fine bubbles on the resistivity ratio is expected to vary with the anode inclination and current density. Compared to the effect of large bubbles, the effect of a change in fine bubbles due to changes in operating conditions on the resistivity ratio appears to be of secondary importance. For the range of coverage ratio here, we may assume that the contribution by fine bubbles remains constant. This is substantiated in Fig. 4 which shows that the best fit lines for both the electrolytic cell and the air–water model are essentially parallel to each other despite the fact that in each case, the data cover a range of current density and anode inclination. As shown in Fig. 4 and Table 1, with the electrolytic cell, the results for the graphite anode and the carbon anode are essentially the same, so only data from the graphite anode is considered in the subsequent analysis.

Table 1. $a_{1\,cm}$ and $b_{1\,cm}$ values for the AWM, ECG and ECC

Cell type	*AWM*	*ECG*	*ECC*
$a_{1\,cm}$	1.096	1.410	1.401
$b_{1\,cm}$	1.714	1.602	1.592

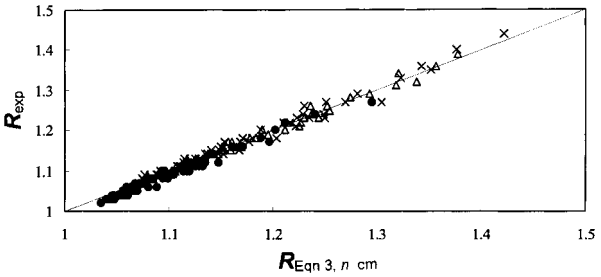

Fig. 5. Comparison between predictions by Equation 3 and the experimental values with $L_{AC} = 3$, 4, 5 and 6 cm and $j = 0.45$, 0.60 and 0.75 A cm^{-2} and electrode inclinations of 2°, 4°, 6° and 8°. Key: (●) AWM, (△) ECG, (×) ECC and (—) Equation 3.

In Fig. 4, by extrapolating the best fit line to zero bubble coverage ratio, the intercept on the ordinate for the ECG is the resistivity ratio due only to the presence of fine bubbles. The intercept on the ordinate for the AWM is the magnitude of the resistivity ratio with no bubbles present, and in theory, this should be equal to unity. The difference in the intercepts between the ECG and the AWM, Δa_{1cm}, is the additional bubble resistivity ratio due to the presence of fine bubbles in the ECG.

$$\Delta a_{1\,cm} = a_{ECG,\,1cm} - a_{AWM,\,1cm} = 0.314$$

where $a_{AWM,1cm}$ and $a_{ECG,1cm}$ are the values of a_{1cm} in the AWM and the ECG, respectively.

Considering Equation 3, it can be shown that

$$\Delta a_{n\,cm} = \Delta a_{1cm}/n = 0.314/n \tag{5}$$

Here, Δa_{ncm} is the additional bubble resistivity ratio for the electrolytic cell at an anode–cathode distance of n cm and zero bubble coverage ratio when compared with that of the AWM.

The total resistance ratio increase due to the existence of the bubble layer under the anode can be estimated from Equation 3 as

$$\Delta R_{n\,cm} = \frac{a_{1cm} - 1}{n} + \frac{b_{1cm} f}{n} \tag{6}$$

Considering that the maximum bubble coverage ratio obtained for the electrolytic cell in this work is 0.278, the additional bubble resistivity ratio $\Delta a_{n\,cm}$ caused by fine bubbles in an electrolytic cell contributed at least 37% of the total resistance ratio increase ΔR_{ncm} due to the existence of the bubble layer. With a

decrease in the bubble coverage ratio, the contribution of fine bubbles increases.

Thus, in comparing an electrolytic cell with an air–water model, the most distinguishing features are the presence of fine bubbles in the former and the fine bubbles contribute significantly to the overall resistance increase.

Although the geometry, the electrolyte properties, the operation temperature and especially the dimensions of anodes used in this work are significantly different from those in an industrial aluminium reduction cell, this work illustrates the existence of fine bubbles during electrolysis and the effect of these fine bubbles on resistance ratio. Thus, great care must be exercised when applying the results from an air–water model to an aluminium reduction cell.

4. Conclusions

The bubble resistivity ratio for horizontal electrodes was investigated in both an air–water physical analogue model and an electrolytic cell. Results showed that at the same current density or equivalent gas generation rate, the difference in the bubble resistivity ratio between the two cells can be up to 20%. Consequently, the results obtained from an air–water model cannot be directly applied to an electrolytic cell, even with an identical geometry.

Within the range of experimental conditions covered, it was shown that the bubble resistivity ratio for a given anode–cathode distance is linearly related to the bubble coverage ratio for both the air–water model and the electrolytic cell; and in the electrolytic cell, it is also true for both the graphite anode as well as the carbon anode, the two anode materials tested in this work.

By extrapolating the bubble resistivity ratio to zero bubble coverage, the effect of fine bubbles on the bubble resistivity ratio was investigated and shown to be a significant part of the total resistance increase.

References

[1] W. E. Haupin, *in* 'Production of Aluminium and Alumina', 2nd edn (edited by A. R. Burkin), John Wiley & Sons, Chichester (1987), pp. 150–58.

[2] G. J. Houston, M. P. Taylor, D. J. Williams and K. Grjotheim, Predicting bath properties in aluminium smelting electrolysis, *in* 'Light Metals' (Edited by L. G. Boxall), TMS 117th Annual Meeting, Phoenix, AZ (1988), pp. 641–45.

[3] L. J. J. Jolas and J. Bos, Cathode drop comparison on aluminium Pechiney modern cells, *in* 'Light Metals', (edited by U. Mannweiler), TMS 123 Annual Meeting, San Francisco, (1994), pp. 403–13.

[4] R. C. Dorward and J. R. Payne, Development of monolithic titanium diboride cathodes for retrofit Hall cell applications, *in* Topic Report for US Department of Energy, DE AC07-76CS40215 (1983).

[5] A. Solheim and J. Thonstad, Model cell studies of gas induced resistance in Hall–Héroult cells, *in* 'Light Metals' (edited by R. E. Miller), TSM 115th Annual Meeting, New Orleans, LA (1986), pp. 379–403.

[6] R. Shekhar and J. W. Evans, Modelling studies of electrolyte flow and bubble behaviour in advanced Hall cells, *in* 'Light Metals' (edited by C. M. Bickert), TMS 119th Annual Meeting, Anaheim, CA (1990), pp. 243–8.

[7] D. Kasherman and M. Skyllas-Kazacos, *J. Appl. Electrochem* **18** (1988), pp. 863–8.

[8] R. Dorin and E. J. Frazer, *ibid.* **23** (1993), pp. 933–42.

[9] J. Xue and H. A. Øye, Bubble behaviour – Cell voltage oscillation during aluminium electrolysis and the effects of sound and ultrasound *in* 'Light Metals' (edited by J. W. Evans), TMS 124th Annual Meeting, Las Vegas, (1995), pp. 265–71.

[10] K. Qian, J. J. J. Chen and N. Matheou, *J. Appl. Electrochem.* **22** (1997), pp. 434–40.

[11] D. A. G. Bruggeman, *Ann. Phys.* **24** (1935), 636–64.

[12] F. Hine and K. Murakami, *J. Electrochem. Soc.* **127**(2) (1980), 292–7.

[13] H. Vogt, *Electrochim. Acta*, **26** (1981) 1311–17.

[14] P. J. Sides and C. W. Tobias *J. Electrochem. Soc.* **129**(12) (1982) 2715–20.

[15] R. C. Dorward, *J. Appl. Electrochem.* **13** (1983) 569–75.